ADVANCED INTELLIGENT SYSTEMS
Open Access
www.advintellsyst.com

Unobtrusive, Low-Cost Out-of-Hospital, and In-Hospital Measurement and Monitoring System

Tiina Vuorinen, Kai Noponen, Vala Jeyhani, Muhammad Awais Aslam, Matti Juhani Junttila, Mikko Paavo Tulppo, Kari Sakari Kaikkonen, Heikki Veli Huikuri, Tapio Seppänen, Matti Mäntysalo, and Antti Vehkaoja*

Continuous monitoring of vital signs can be a life-saving matter for different patient groups. The development is going toward more intelligent and unobtrusive systems to improve the usability of body-worn monitoring devices. Body-worn devices can be skin-conformable, patch-type monitoring systems that are comfortable to use even for prolonged periods of time. Herein, an intelligent and wearable, out-of-hospital, and in-hospital four-electrode electrocardiography (ECG) and respiration measurement and monitoring system is proposed. The system consists of a conformable screen-printed disposable patch, a measurement unit, gateway unit, and cloud-based analysis tools with reconfigurable signal processing pipelines. The performance of the ECG patch and the measurement unit was tested with cardiac patients and compared with a Holter monitoring device and discrete, single-site electrodes.

1. Introduction

Cardiovascular diseases (CVDs)-related deaths (17.9 million deaths in 2016) are the most common causes of death and their number is rapidly increasing due to growth and aging of population, changes of living habits, and other epidemiologic factors. Identifying the people at the highest risk of CVDs and making sure that they receive proper treatment and monitoring can prevent premature deaths.[1,2] Both out-of-hospital and in-hospital cardiac monitoring for risk groups are needed to improve this global problem.

Traditional body monitoring systems have bulky electrodes, wires, connectors, and stationary or portable separate central units. The development is currently going toward more unobtrusive patch-type monitoring systems to improve usability and comfortability.[3–5] In addition, energy-storage and harvesting issues are important research topics in a field of wearable electronics.[6–8]

A lot of research is done in the field of wearable systems and cardiac disease monitoring.[9,10] ECG devices can be classified, for example, by the number of leads they are measuring, and the 12-lead ECG is considered as the standard practice to asses cardiac activity.[11] In a single-lead system one electrode pair ("lead") records the heart activity. As an example, Pradhan et al. studied ambulatory arrhythmia detection with single-channel ZIO XT Patch in pediatric patients and compared it with a regular Holter monitor.[12] Other patch-type single-lead devices are for example NUVANT and CAM.[13,14] There are also single-lead devices, such as AliveCor and ECG Check, that utilize a separate sensor unit that measures the ECG from the fingertips.[15,16] Proesmans et al. studied a mobile phone-based use of the photoplethysmography technique to detect atrial fibrillation in primary care.[17]

In multilead systems several leads record the cardiac activity signals. As a result, the multilead systems provide more information from different angles of the heart. Lin et al. developed an artificial intelligence of things (AIoT) system for ECG analysis and cardiac disease detection.[18] In their study they used conventional wire-connected electrodes and an ECG-sensing device with 84.55 mm × 39.38 mm × 18.31 mm dimensions. Mishra et al. proposed a three-lead wearable ECG for real-time P-QRS-T detection and classification of various arrhythmias.[19] The measurement unit consists of conventional electrodes, wires, and a printed circuit board (PCB), and the last two are covered with a casing.

To further improve the possibilities for continuous monitoring of vital signs, we are proposing an intelligent, multilead,

T. Vuorinen, Prof. M. Mäntysalo
Faculty of Information Technology and Communication Sciences
Tampere University
33720 Tampere, Finland
E-mail: tiina.vuorinen@tuni.fi

K. Noponen, M. A. Aslam, Prof. T. Seppänen
Center for Machine Vision and Signal Analysis
University of Oulu
90570 Oulu, Finland

V. Jeyhani, Prof. A. Vehkaoja
Faculty of Medicine and Health Technology
Tampere University
33720 Tampere, Finland

Prof. M. J. Junttila, Prof. M. P. Tulppo, Dr. K. S. Kaikkonen, Prof. H. V. Huikuri
Research Unit of Internal Medicine
Medical Research Center Oulu
University of Oulu and Oulu University Hospital
90570 Oulu, Finland

The ORCID identification number(s) for the author(s) of this article can be found under https://doi.org/10.1002/aisy.202000030.

DOI: 10.1002/aisy.202000030

unobtrusive, low-cost system for both out-of-hospital and in-hospital monitoring. The proposed system follows the iHome Health-IoT concept proposed in a previous study[20] that included three main parts: Health-IoT on body, Health-IoT at home, and Health-IoT in cloud. There is, however, modifications and adaptations based on the observed needs and necessities. In this article, the proposed system has four main parts, which are shown in **Figure 1**. They are 1) measurement unit and printed electrodes, 2) gateway unit, 3) cloud-based data analysis and storing tools, and 4) front-end tools for data viewing and decision-making.

The system is designed with various different applications in mind, the primary ones including in-hospital and in-home clinical purposes. The system is designed for different modes of measurement, each having specific requirements, limitations, and advantages, enabling it to fit into a variety of applications ranging from online patient monitoring to Holter-type ECG data acquisition for post-hoc analysis. The proposed monitoring system was tested with cardiac patients in collaboration with Oulu University Hospital to verify its functionality.

The required duration of monitoring, required number of leads, and utility of real-time monitoring depend on clinical indications. A key benefit of the proposed architecture and system is its ability to accommodate different requirements with various ECG plaster design variations, automated distributed software component deployment changes, and different measurement modes. This makes the monitoring system a versatile tool suitable for various healthcare providers in cases that do not require the full 12-lead ECG due to clinical guidelines and recommendations.

The proposed system can increase the user acceptability, which have been shown[9] to increase study completion rates and clinical yields of arrhythmias diagnoses, for example, for atrial fibrillation due to the longer measurement durations. What is more, the developed electrode plaster with multiple channels and longer intraelectrode distances is able to capture both atrial and ventricular activity, enabling differential diagnosis of arrhythmias as well as other cardiac problems, such as ischemic events. Consequently, this also gives the proposed system the ability to verify the absence of abnormal cardiac findings during a long study period with a high enough certainty. This is also very critical information for correct clinical diagnosis. It should also be noted that the diagonal AS lead (electrode locations are shown in **Figure 2**a) is recommended for exercise

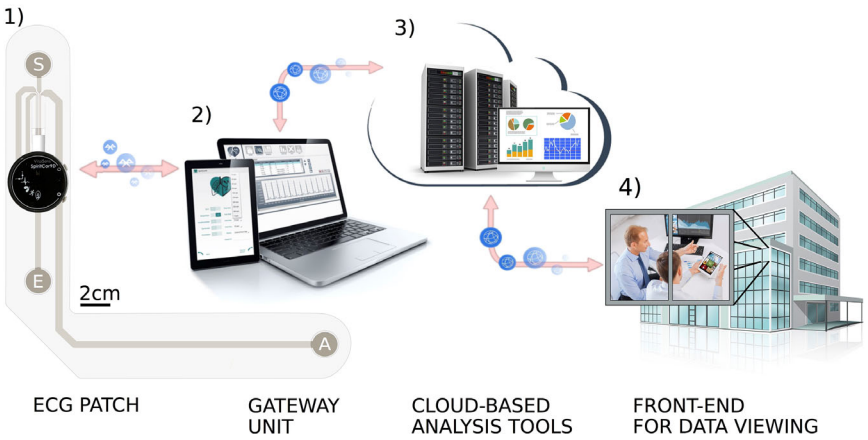

Figure 1. The system architecture that consists of four parts: the measurement unit and the electrode, the gateway unit, the cloud-based data analysis and storing tools, and front-end application for viewing the analysis results in real time or later.

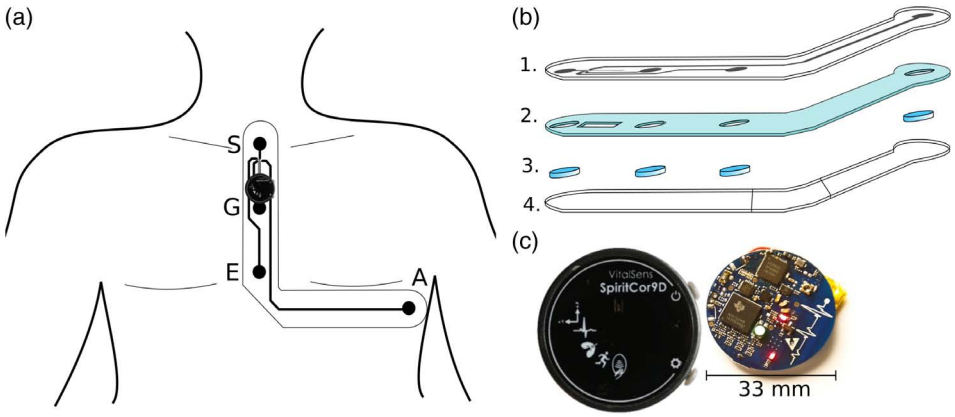

Figure 2. a) An illustration of the patch and the measurement unit in place. b) Electrode patch material layers. 1. thermoplastic polyurethane, 2. silicone adhesive, 3. hydrogel, and 4. PET supportive layer. c) The measurement unit and its PCB.

testing, as it has high sensitivity for exercise-induced ischemia detection.[21–23] Hence, the presented system is also very applicable for ambulatory measurements with physical activity and exercise testing for which it has been separately validated.[24] Both the tolerance to motion-related artifacts and the possibility for lead-off detection with the impedance measurement lessen the false-alarm burden (e.g., pause and asystole). This has been identified as one of the key issues leading to sentinel events in the hospital setting.[25]

2. System Architecture

The measurement unit is responsible for signal acquisition, simple and low-level processing, and finally transmitting the measured data. The measurement unit is also able to store the data if needed. The unit is equipped with a flexible electrode bandage that provides a comfortable and consistent measurement of biosignals.

The gateway unit acts as a bridge between the measurement unit and the cloud-based analysis tools. Compared with the measurement unit, the gateway unit has a much more extensive processing power, battery resource, and various wireless communication technologies to satisfy the more complicated and demanding needs of the data-transmitting tunnels to the cloud. The connection between the measurement unit and the gateway unit is wireless. S2 shows the operation principles of the measurement unit and the graphical user interface in the mobile gateway unit.

The cloud provides data management solutions, which are essential to make it user-friendly and simple for interaction by medical experts, nurses, and patients. It also hosts powerful, reliable, and scalable signal processing pipelines to analyze the recorded data. The results are transferred and visualized to the related medical administrators in a well-managed and illustrative way. Depending on the application they can also be relayed back to the user.

As already said, the system is designed to work in different measurement modes to enable efficient use in different applications. The system can be used for real-time data viewing (only sending the data to the gateway) or only storing the data in the measurement unit. But it can be also used for both storing and transmitting or only transmitting and storing on the cloud.

2.1. Electrode Patch

Figure 2a shows the patch and measurement unit secured in place for monitoring. The electrode patch has four electrodes according to the EAS electrode system. EAS is a subset of the EASI electrode system that is a reduced lead system used mainly by Phillips in their cardiotelemetry systems. ECG recorded with EASI system is often mathematically converted to regular 12-lead ECG signals.[26] The electrode S is located on the manubrium, E is located on the lower part of the sternum, and A on the standard V5 electrode location of the 12-lead system. The electrode potentials are measured with respect to the common reference electrode G (between S and E) and three bipolar leads are formed as potential differences between the electrode sites S, E, and S. These electrode patches were previously tested for movement artifacts and long-term wearability.[24,27]

Figure 2b shows the layer structure of the electrode patch. Layer 1 is thermoplastic polyurethane with silver and silver/silver chloride prints. Silicone adhesive (layer 2) provides firm adherence to the skin and circle-shaped hydrogel patterns ensure good signal quality. Layer 4 is a supportive PET film that will both protect the silicone adhesive layer and help in the installation of the electrode to a measurement subject. The PET film has two cuts so that the electrode patch can be put in place section by section and it is removed when applying the sensor.

2.2. Wireless Technologies

Bluetooth low energy (BLE), also referred to as Bluetooth Smart, is used as the wireless technology between the measurement and the gateway units. BLE offers a suitable power consumption profile for ambulatory devices and the data bandwidth still satisfies the needs of this work and also most other telemonitoring applications. The topology of BLE allows a multiconnection between a central device (a handheld device in this work) and several peripherals (measurement units in this work), meeting the needs of the proposed architecture.

BLE features different approaches to overcome the security problems in the wireless communication, among which, Out of Band (OOB) pairing satisfies the requirements in this application. OOB uses a different wireless technology such as Near Field Communication (NFC) to exchange the Term Key (TK) to encrypt the data. The TK in this pairing method can be up to128 bits, significantly enhancing the security of the connection. As a result, assuming that the OOB channel is protected from man-in-the-middle (MITM) attacks and passive eavesdropping, the connection is also immune to those attacks. In addition, BLE is able to change the device address periodically to overcome the identity-tracking problems.

Additional benefit of BLE is its good tolerance for interference from other radios possibly located in the same space (in-home environment includes mainly WiFi) and operating in the same 2.4 GHz frequency band. Three advertising channels of BLE that are used in forming of a connection are located outside and between the WiFi channels and due to the frequency-hopping communication scheme (changing of the communication channel for each connection interval, i.e., tens of times per second) the data transmission is not compromised even though additional radio traffic would exist in the same frequencies.

The UART service is utilized for sending the raw data from the measurement device to the gateway unit. This service is able to transfer up to 20 bytes of data in one packet. Depending on the receiving device, there may be up to six packets sent in one BLE connection interval, which can be set as short as 7.5 ms. This sets the maximum theoretical limit for the rate of transmitted data when not considering the packet retransmissions. The structure of the 20-byte packet varies depending on the nature of the information being transmitted, being either command packets or data packets. The data packets, in addition to the actual data, include packet header and packet counter. Therefore, the central device is able to recognize which channel of data is received and if any packet has been dropped.

The command packets are used to transfer measurement configurations, status, and other types of information that concern the user. The measurement configuration consists of the settings selected by the user in interaction with the gateway device prior to starting the measurement. Settings such as the mode of the measurement, enabled channels and sensors, and selected data rate for each enabled channel are included in the configuration packet. Additionally, this type of packet includes some other information such as the time, date, and the subject ID.

The status packet is transmitted periodically to report the status of the measurement device to the gateway unit. Information such as battery level, status of lead-off detection flags, and number of BLE packets left in the buffer are sent via the status packet.

The nature of BLE brings a good level of compatibility with other devices. For instance, inclusion of the heart rate service in the measurement unit enables it to communicate directly with Android and iOS sports applications (assuming that the underlying hardware of the handheld device supports BLE). However, the self-defined data structure in the UART service limits the compatibility in sending the raw measurement data to other gateway unit software, which do not implement the same data structure.

2.3. Gateway Unit

The gateway unit can play different roles in the described architecture. For applications such as in-home monitoring, a handheld device such as a smartphone or a tablet is a beneficial choice. Using these devices, which are currently an inseparable part of our lives, not only is the cost of the system reduced but also the user adaptation to the system is simplified. Additionally, the handheld devices nowadays are equipped with powerful features and computing capabilities, which may be utilized in the system with only designing an app.

In this work, an Android application was designed that makes use of the BLE module of the mobile device to transmit and receive data from the measurement unit. The user configuring the monitoring system is able to choose the mode of the measurement and customize it according to her/his needs. Depending on the selected mode, the software is able to monitor the measured signals in real time, along with other useful information such as battery level.

2.4. Measurement Unit

The measurement device includes an nRF52832 Microcontroller Unit (MCU), which has a powerful BLE capable radio module and integrated BLE protocol stack. It also has a 32-bit ARM Cortex-M4F processor, 512 kB of flash memory and 64 kB of RAM, on-chip NFC unit, and several peripherals, which are required for the device, e.g., counters and analog-to-digital converters.

In this study, the device is used to measure three channels of ECG and impedance pneumography (IP). In addition, it can be used to record three channels of accelerometers and three channels of gyroscope signals. This is a combination that is not currently available in any of the commercial small-sized wearable monitoring devices, to the best of our knowledge. The three channels of ECG can be utilized in measuring the EASI lead set or a subset of the standard 12-lead ECG e.g., limb leads and one channel of the chest leads. The IP signal is simultaneously measured through two of the ECG electrodes. The ECG and IP acquisition are powered by the ADS1294R analog-front-end circuit from Texas Instruments, providing additional features such as pacemaker detection, Central Wilson Terminal calculation, lead-off detection, and right-leg drive.

The electrode patch is connected to the device through a micro USB connector. The same connector is also used for connecting the measurement unit to a computer when extracting locally stored data and for charging it. A memory of two gigabytes is embedded in the device. The data structure is strictly controlled by the MCU to provide reliable and fast read and write processes. According to the designed data structure for the local memory, an empty memory can hold up to 5.4 days of measurement data including three channels of ECG with a data rate of 500 samples per second and a resolution of 24 bits. Obviously, the number of enabled channels, their resolution, and data rate have a direct impact on the amount of consumed memory per a unit of time.

Figure 2c shows the measurement unit and its PCB. The unit has a circular shape with a diameter of 33 mm and the PCB consists of 4 layers and about 200 components. The tallest components on the top and bottom layers have a height of 1.83 and 2.51 mm, which are a red-green-yellow light-emitting diode (LED) and the micro USB connector. The PCB weighs 3.7 g with all the components assembled (except the battery), including an SD card. The total weight including a prismatic 300 mAh battery and the enclosure is 13.4 g.

The power consumption of the device naturally varies according to the measurement mode used and the number of measured signals. When all the measurement channels are activated and the data are both stored locally and transmitted over BLE, the average current consumption is 8.62 mA and the battery lifetime is approximately 35 h. When operated as a Holter device i.e., only ECG is measured and the data are stored locally, the battery lifetime extends to more than 100 h.

3. Preliminary Evaluation of Measurement Performance

To assess the quality of the measured ECG signal, lead II of the standard 12-lead system was measured simultaneously by two devices: the developed device and Faros 360 Holter device manufactured by Bittium Biosignals Ltd. Two pairs of electrodes were placed as close as possible to each other, one pair on the right forearm and one on the left ankle. The sampling rate in both of the devices was set to 1000 samples per second. Another test was made to compare the internal noise of the two devices by attaching the measurement input terminals together. In Faros device, a 196 kΩ resistance was connected between the inputs to emulate the fault current limiting series resistance of its electrode cables. In the proposed device this series resistance is built inside the device.

Figure 3 shows the result of the measurements. The signal measured with the developed device shows an equal quality in comparison with the reference device. The offset in the signal of the developed device (Figure 3d,e) is due to a difference in

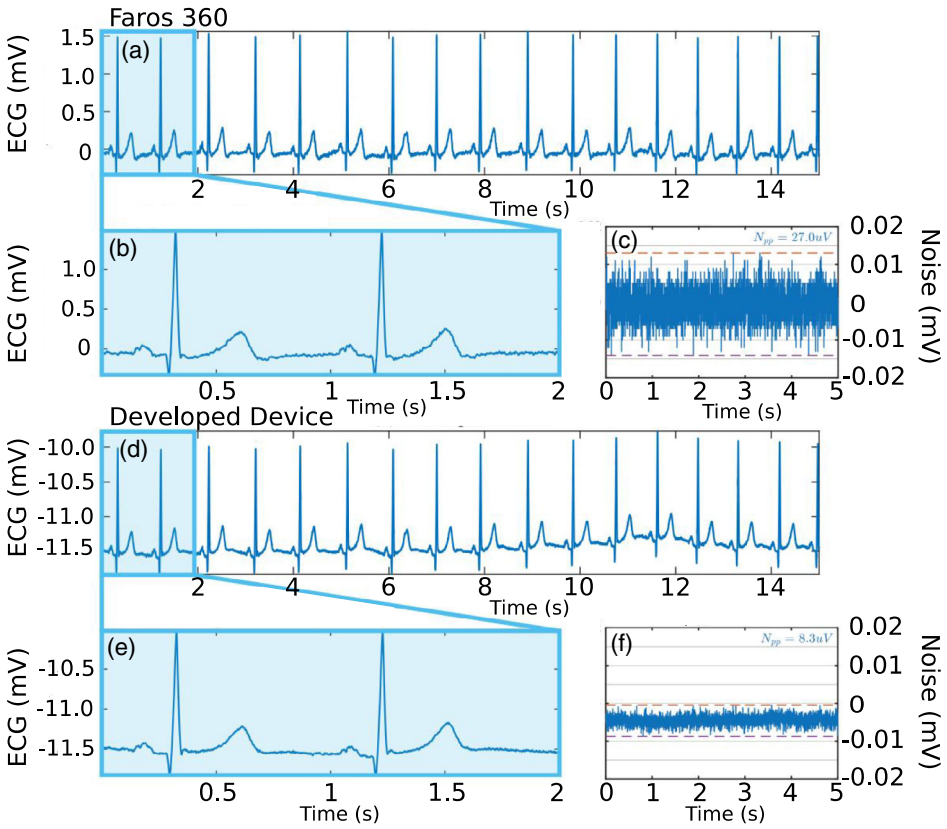

Figure 3. a–c) Signal quality comparison between Faros 360 and d–f) the developed measurement device.

the half-cell potential of the measurement electrodes and the absence of any high-pass filtering of the measurement signal. The approach of not removing the baseline before the analog-to-digital conversion is advantageous as more powerful digital filtering methods can be used, which are able to preserve the desired low-frequency signal components' better analog filters. Figure 3c,f shows the internal noise signal of the two devices. About 8.3 μV peak-to-peak noise voltage was measured for the proposed device, which is over two-thirds smaller than 27.0 μV measured for the reference device. The difference is likely caused by different design choices and components used in the two devices but more accurate evaluation is not possible as the internal structure and components used in the commercial device are not public information.

Another test was made to optimize and verify the performance of the IP measurement. First, the coupling of cardiac components to the impedance signal was minimized by testing various excitation frequencies and measurement phase combinations in a measurement setting where electrodes were placed on V6 and VR6 locations. Excitation frequency of 32 kHz and phase of 67.5° were found as the optimal combinations. An example of the respiration signal measured with the aforementioned settings is shown in **Figure 4**. To evaluate the measurement signal, flow thermography was also performed simultaneously by a negative temperature coefficient (NTC) thermistor placed inside a breathing mask that was worn in front of the mouth and nostrils. The original measured IP signal and its filtered version are shown in the first and second panels, respectively. The third panel illustrates the output of the NTC thermistor. The used filter was a band-pass infinite impulse response (IIR) filter with cut-off frequencies of 0.06 and 1 Hz, applied by the forward–backward technique. The quality of the filtered signals compared well with the quality of the gold standard flow thermography reference. The respiration rates calculated from the two signals are 10.68 and 10.64 breaths per minute. The advanced counting method proposed by Jeyhani et al. was utilized for estimating the respiration cycle length.[28]

4. Signal Processing and Cloud Service Architecture

We developed a scalable monitoring platform architecture for distributed signal processing. This enables efficient, reliable, and robust extraction of clinical markers from biosensor data in the presence of noise and artefacts stemming from the uncontrolled remote monitoring context. The architecture encompasses the whole system (measurement unit, gateway, and cloud) and is organized into configurable distributed pipelines of software components. The pipelines represent computational chains, e.g., starting from raw measurement data up to a specific arrhythmia alarm. The individual computational software components of the pipeline can be deployed on the wearable unit, the gateway, and/or the cloud as needed. This makes the system intelligently capable of adapting to the expectations, as also the

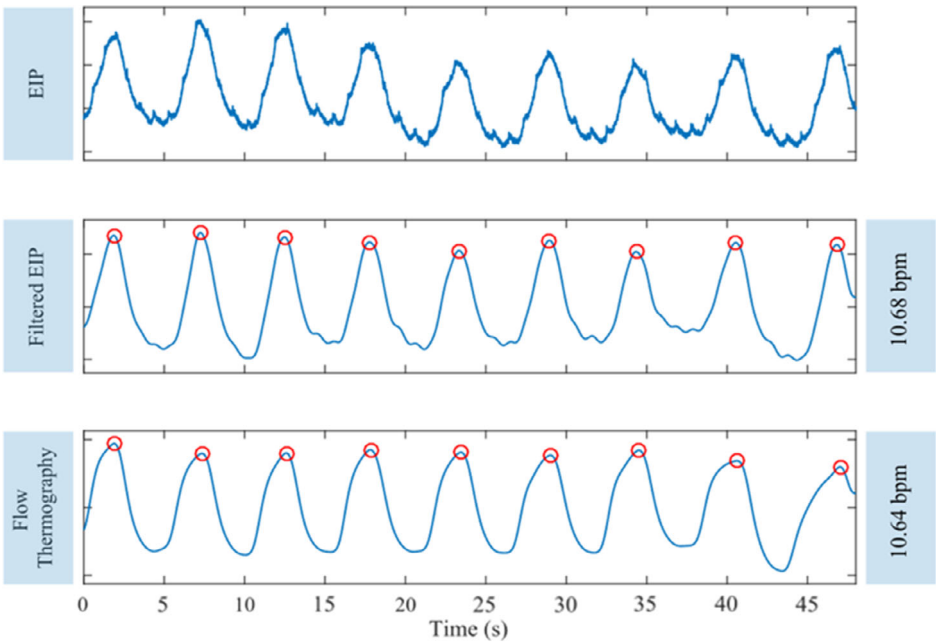

Figure 4. IP signal measured with the proposed device in comparison with a gold standard flow thermography signal.

different pipeline configurations can be activated and automatically configured at will based on the clinical needs, to achieve desired quality of service and optimize power consumption and communication costs. The adaptation occurs via use case rules that activate predefined sets of components and set their parameters accordingly. This eases the setup procedure and facilitates large-scale deployment of the system for the masses. The components are interchangeable pieces of executable software that can be implemented in any suitable programming language and that communicate through the tcp/ip stack via predefined protocols, allowing for distributed deployment.

A working implementation of the platform was created using Python language. In this instance, all the signal processing pipelines for real-time remote ECG monitoring are deployed on the cloud service and interfaced by the signal routing component running on the gateway device. We used Web Application Messaging Protocol (WAMP) as a middleware solution to interconnect the software components. It is an open standard web socket protocol having implementations in Autobahn framework and Crossbar router which we also utilized. The utilization of WAMP and real-time performance considerations in ECG monitoring are described in more detail in a previous study.[29] The implemented signal processing pipelines detect heartbeats and extract the R-peak locations from the ECG, classify the beats, and calculate RR-interval tachogram signal and heart rate variability (HRV) features. There are also pipelines to detect arrhythmias such as pauses or asystoles, brady- and tachycardias, and atrial flutter or fibrillation categorized into three different levels of severity. These three categories are the following: green for suspected single-time events, yellow for potentially dangerous, and red for life critical events. Examples of previous categories are shown and described in **Table 1**.

The gateway unit sends the raw data from the measurement unit to the cloud where it is processed by the aforementioned computational pipelines. Next, the relevant results are returned back to the gateway device in a reasonable amount of time (in a couple of seconds). Some of the results are also transmitted to the physicians and nurses responsible for the ongoing

Table 1. Examples of arrhythmia diagnoses rules and respective alarm ratings.

Red alarms	Yellow alarms	Green alarms
HR exceeds 240 bpm for longer than 4 s, Ventricular fibrillation is diagnosed and red alarm is raised.	Average HR over 160 bpm, extreme tachycardia is diagnosed, and yellow alarm is raised.	Average HR of three consecutive beats lower than 40 bpm, bradycardia is diagnosed, and green alarm is raised.
Three consecutive ventricular beats with HR over 120 bpm, ventricular tachycardia is diagnosed, and red alarm is raised.	Average HR under 35 bpm, severe bradycardia is diagnosed, and yellow alarm is raised.	Three consecutive ventricular beats with HR under 120 bpm, ventricular rhythm is diagnosed, and green alarm is raised.
RR-interval of two consecutive beats is more than 4 s, asystole is diagnosed, and red alarm is raised.	–	RR-interval of two consecutive beats is more than 2 s, pause is diagnosed, and a green alarm is raised.

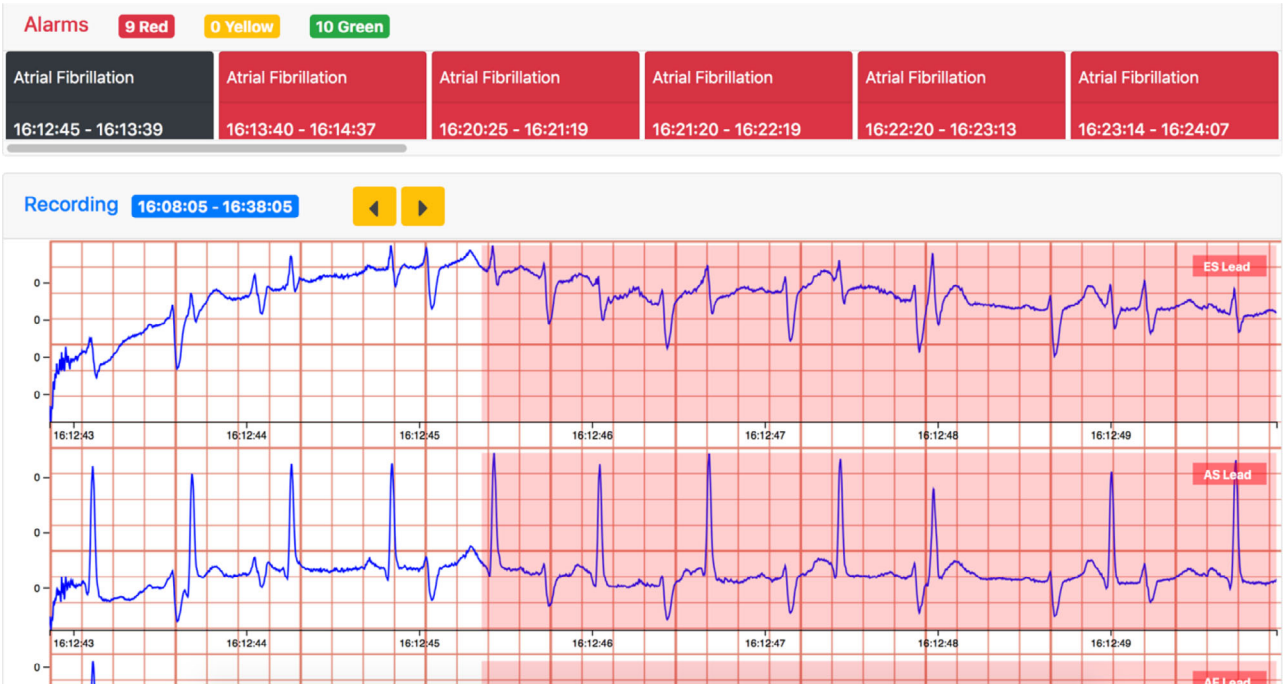

Figure 5. A sample view of the web browser-based GUI for viewing the ECG data the cloud service.

measurement. Additionally, the outcomes of the pipeline analyses along with the raw data are stored in a database in the cloud. **Figure 5** shows the cloud service user interface implemented for data viewing. A test case is presented wherein supraventricular tachycardia is progressing into atrial fibrillation and the atrial fibrillation alarm is raised from the onset of arrhythmia.

5. Clinical Testing

The monitoring system was tested at Oulu University Hospital, with eight volunteers (two females, six males), as a substudy of ESCAPE-Part-II study (Clinical Utility of Home Monitoring of Electrocardiogram and other Vital Functions). The primary objectives of ESCAPE-Part-II research project were to examine the effects of exercise training on glucose control and cardiac autonomic function in patients with impaired glucose tolerance. There were no significant arrhythmias in the data of the subjects, which, however, was not unexpected as they were chosen based on glucose control to the study. There were premature ventricular contractions (PVCs) especially in subject three, but no other ventricular arrhythmias or atrial fibrillation. Overall, the proposed system could confirm the absence of aberrancy similarly to the analysis of the Faros 360 data.

A comparison of the signal quality in the ambulatory clinical use case was performed posthoc. QRS complexes were detected

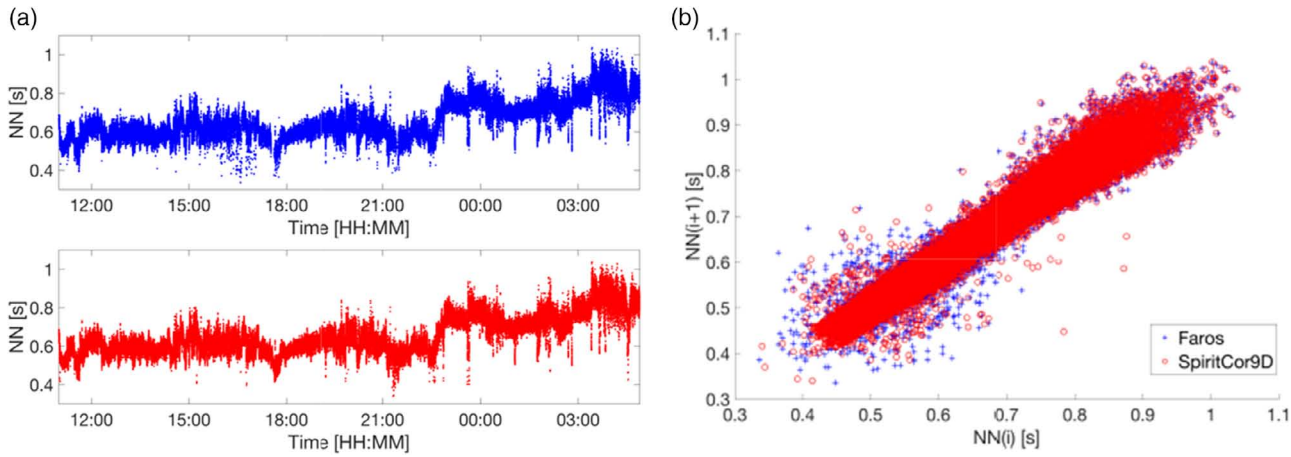

Figure 6. a) NN-tachograms of Faros 360 (top) and measurement unit (bottom) for the subject one. b) Superimposed Poincaré plots of the NN beats from Faros 360 (blue +) and measurement unit (red circle) for the subject one.

from the magnitude signal from both devices using the R-peak detector implemented in the data analysis pipeline. The sampling rate of the developed device was set to 500 Hz during the long-term recording, to save storage space. Faros 360 data were upsampled with cubic splines from 250 to 500 Hz to match the sampling rate used in the proposed device. The magnitude signals were formed as the square root of the sum of squared channels after baseline wander removal with a zero-phase digital high-pass filter (0.67 Hz cutoff). Deviating beats and intervals were automatically filtered out from the RR-interval series by the following rules: the interval differs by more than 13.5% from the ten-beat average or R-peak amplitude is higher than 1.5 mV. Overall, the Faros 360 signal was more prone to noise for example due to the movement of cabling. This led to the removal of 5.9% of the Faros 360 RR-intervals compared with that of 1.4% of the measurement unit RR-intervals for subject one. Removed beats included ectopic beats such as PVCs and noise artefact detections. The larger amount of artefact signal in the commercial system may be due to the cabling of the individual electrodes being more influenced by movement and being more susceptible to tangling to clothing. **Figure 6**a shows the resulting NN-intervals of the subject one, and in Figure 6b the corresponding Poincaré plots are overlaid on each other to show the agreement between the consecutive intervals.

Over the course of the concurrent 24 h measurements, the clock rate(s) of either of the two devices or both of them wandered slightly with respect to each other when comparing the tachograms closely. Nevertheless, a good overall agreement can be seen from the plot shapes of Figure 6, and the clear similarity over the short-time durations is witnessed in Figure 6b.

6. Conclusion

In this study, the developed unobtrusive measurement and monitoring system is used to measure and record three channels of ECG and IP using a comfortable ECG patch. These recordings can provide extensive information on a person's health and also on the measurement context, helping to arrive at the correct diagnosis. Performed clinical tests indicate that the system provides HRV analysis capability comparable with and even exceeding the performance of a commercially available product conforming to medical device standards. They also indicate that the plaster ECG can be less susceptible to motion artifacts than conventional electrodes using cabling, leading to the reduced rate of artifact beats.

There are many use cases for the proposed system. According to expert consensus, ambulatory ECG (AECG) monitoring can be recommended either for diagnosis or for risk stratification in patients with for example unexplained syncope or palpitations, atrial fibrillation, Wolf–Parkinson–White syndrome, cryptogenic stroke, newly diagnosed nonischemic cardiomyopathy or hypertrophic cardiomyopathy, arrhythmogenic right ventricular dysplasia, and after acute myocardial infarction or with a healed myocardial infraction and borderline ejection fraction.[9] It is also recommendable in monitoring the efficacy of arrhythmia suppression, especially with outpatient initiation of antiarrhythmic drugs, and to detect adverse drug responses.[30] The proposed system could be used in the hospital setting in scenarios wherein telemetry with reduced lead sets is warranted for arrhythmia or ST-level monitoring, for example, according to the American Heart Association (AHA) recommendations.[25]

We see that the proposed system for remote monitoring of vital functions is especially intriguing in the context of clinical practice. Currently, medical staff is under pressure to further shorten the hospitalized inpatient times, and relocation of patients to step-down units such as patient hotels has been discussed. Patient care in these step-down units can be made possible with such innovations expanding remote monitoring systems to patient hotels and ultimately to domestic environments in the future. In addition, the possibilities of the proposed kinds of systems in noncardiac units, such as orthopedic, should be explored further.

In the future, the user comfort could be improved with more conformable substrate materials that would also enable longer wearing time for the electrode patch. If this could be combined with a lower power consumption, the lifetime of the system could be prolonged up to a week or even to a month. In addition, extending the range of signal processing algorithms and diagnosis tools would enable the use of the system in a wider range of applications.

7. Experimental Section

Sample Fabrication: The manufacturing process as well as the material choices were designed in collaboration with Screentec Ltd. that produced the bandages according to our design and instructions. Circular electrode

Table 2. Subject demographics.

Gender	Age [year]	Height [cm]	Weight [kg]	SBP [mmHg]	DBP [mmHg]	Hba1C [mmol mol]	Diabetes medication	BP medication
F	50	155	83	111	85	37	Yes	No
M	56	175	93	137	103	43	No	No
M	55	180	123	126	81	42	No	Yes
M	53	178	117	160	112	42	Yes	No
M	59	175	106	125	82	43	No	No
F	53	161	98	134	91	54	Yes	Yes
M	54	178	98	130	80	41	No	No
M	57	175	94	149	95	37	Yes	No
	54.6 ± 2.8	172.1 ± 9.0	101.4 ± 13.3	134.0 ± 15.1	91.1 ± 11.6	42.4 ± 5.3		

areas were screen printed using CI-4040 stretchable Ag/AgCl ink (ECM) and the circuitry was screen printed with stretchable silver ink. Ag/AgCl ink contained 40–50 wt% silver powder and 5–15 wt% silver chloride powder diluted in diethylene glycol ethyl ether acetate solvent. Printing was done on a 125 μm-thick stretchable thermoplastic polyurethane substrate (T 391, Policrom Screens) and the pattern was annealed in a convection oven after printing. A silicone adhesive layer was placed on top of the print and circular hydrogel pieces were placed at the electrode locations. In addition, the adhesive layer was used to attach the bandage to the skin. The used adhesive layer was so strong that normal body movements such as arm swing or rotation of upper body did not influence adhesion. Round-shape pieces of 0.89 mm-thick AG635 sensing gel (Axelgaard) were used at the electrode–skin interface to form a stable electrical contact.

Clinical Testing: Concurrent measurements were made with the measurement unit and a three-channel Faros 360 device. Chest hair was shaved prior to the recordings underneath the bandage. Next the skin was wiped with alcohol and dead skin cells were scraped off with Red Dot prep tape (3M). The bandage was then fixed in place and a data recording device attached to the bandage with a micro-USB connector. Flexifix adhesive film was used to secure the device in place and minimize any mechanical stress to the micro-USB connector. A similar process was followed to attach the Faros 360 electrodes but additionally the cabling was secured with skin tape. The recording was turned on and the participant was able to go home for the next 24 h. The recording stopped automatically after 24 h and patients returned the devices at the next day. **Table 2** shows the characteristics of the eight subjects who participated in this substudy.

The study was performed according to the Declaration of Helsinki, and the local committee of research ethics of the Northern Ostrobothnia Hospital District approved (#88/2015) the protocol and all the subjects provided written informed consent.

Supporting Information

Supporting Information is available from the Wiley Online Library or from the author.

Acknowledgements

This work was funded by the Finnish Funding Agency for Technology and Innovation (Tekes) as a part of project VitalSens (decision ID 40103/14) and ESCAPE (618/31/2015) and Academy of Finland (grant nos. 288945, 292477, 318927, and 319408). T.V. thanks KAUTE Foundation and Eemil Aaltonen Foundation for support. K.N. would like to thank Tauno Tönning Foundation for support.

Conflict of Interest

The authors declare no conflict of interest.

Keywords

body-worn monitoring, electrocardiography, impedance pneumography, printed electronics, wireless monitoring

Received: February 25, 2020
Revised: March 27, 2020
Published online:

[1] G. A. Roth, M. H. Forouzanfar, A. E. Moran, R. Barber, G. Nguyen, V. L. Feigin, M. Naghavi, G. A. Mensah, C. J. L. Murray, *N. Engl. J. Med.* **2015**, *372*, 1333.
[2] W. H. O. (WHO), *World Health Statistics 2018: Monitoring Health for the SDGs, Sustainable Development Goals*, WHO, Geneva **2018**.
[3] D.-H. Kim, N. Lu, R. Ma, Y.-S. Kim, R.-H. Kim, S. Wang, J. Wu, S. M. Won, H. Tao, A. Islam, K. J. Yu, T.-i. Kim, R. Chowdhury, M. Ying, L. Xu, M. Li, H.-J. Chung, H. Keum, M. McCormick, P. Liu, Y.-W. Zhang, F. G. Omenetto, Y. Huang, T. Coleman, J. A. Rogers, *Science* **2011**, *333*, 838.
[4] W.-H. Yeo, Y.-S. Kim, J. Lee, A. Ameen, L. Shi, M. Li, S. Wang, R. Ma, S. H. Jin, Z. Kang, Y. Huang, J. A. Rogers, *Adv. Mater.* **2013**, *25*, 2773.
[5] Y. Liu, M. Pharr, G. A. Salvatore, *ACS Nano* **2017**, *11*, 9614.
[6] Y. Zou, P. Tan, B. Shi, H. Ouyang, D. Jiang, Z. Liu, H. Li, M. Yu, C. Wang, X. Qu, L. Zhao, Y. Fan, Z. L. Wang, Z. Li, *Nat. Commun.* **2019**, *10*, 2695.
[7] B. Shi, Z. Liu, Q. Zheng, J. Meng, H. Ouyang, Y. Zou, D. Jiang, X. Qu, M. Yu, L. Zhao, Y. Fan, Z. L. Wang, Z. Li, *ACS Nano* **2019**, *13*, 6017.
[8] H. Ouyang, Z. Liu, N. Li, B. Shi, Y. Zou, F. Xie, Y. Ma, Z. Li, H. Li, Q. Zheng, X. Qu, Y. Fan, Z. L. Wang, H. Zhang, Z. Li, *Nat. Commun.* **2019**, *10*, 1821.
[9] E. Fung, M.-R. Järvelin, R. N. Doshi, J. S. Shinbane, S. K. Carlson, L. P. Grazette, P. M. Chang, R. S. Sangha, H. V. Huikuri, N. S. Peters, *Front. Physiol.* **2015**, *6*, 149.
[10] L. Y. Chen, N. S. Roetker, A. R. Folsom, A. Alonso, S. R. Heckbert, *Circulation* **2015**, *132*, A11721.
[11] P. Guzik, M. Malik, *J. Electrocardiol.* **2016**, *49*, 894.
[12] S. Pradhan, J. A. Robinson, J. K. Shivapour, C. S. Snyder, *Pediatr. Cardiol.* **2019**, *40*, 921.
[13] J. M. Engel, V. Mehta, R. Fogoros, A. Chavan, in *Annual Int. Conf. of the IEEE Engineering in Medicine and Biology Society*, IEEE, San Diego, CA **2012**, pp. 2440–2443.
[14] W. M. Smith, F. Riddell, M. Madon, M. J. Gleva, *Am. Heart J.* **2017**, *185*, 67.
[15] J. P. J. Halcox, K. Wareham, A. Cardew, M. Gilmore, J. P. Barry, C. Phillips, M. B. Gravenor, *Circulation* **2017**, *136*, 1784.
[16] H. T. Haverkamp, S. O. Fosse, P. Schuster, *Indian Pacing Electrophysiol. J.* **2019**, *19*, 145.
[17] T. Proesmans, C. Mortelmans, R. Van Haelst, F. Verbrugge, P. Vandervoort, B. Vaes, *JMIR Mhealth Uhealth* **2019**, *7*, e12284.
[18] Y. Lin, C. Chuang, C. Yen, S. Huang, P. Huang, J. Chen, S. Lee, in *IEEE Biomedical Circuits and Systems Conf.* IEEE, Nara **2019**, pp. 67–70.
[19] B. Mishra, N. Arora, Y. Vora, in *11th International Conference on Communication Systems & Networks*, IEEE, Bengaluru **2019**, pp. 870–875.
[20] G. Yang, L. Xie, M. Mäntysalo, X. Zhou, Z. Pang, L. D. Xu, S. Kao-Walter, Q. Chen, L. Zheng, *IEEE Trans. Ind. Informatics* **2014**, *10*, 2180.
[21] G. F. Fletcher, P. A. Ades, P. Kligfield, R. Arena, G. J. Balady, V. A. Bittner, L. A. Coke, J. L. Fleg, D. E. Forman, T. C. Gerber, M. Gulati, K. Madan, J. Rhodes, P. D. Thompson, M. A. Williams, *Circulation* **2013**, *128*, 873.
[22] M. Puurtinen, T. Nieminen, M. Kähönen, T. Lehtimäki, R. Lehtinen, K. Nikus, J. Hyttinen, J. Viik, *Clin. Physiol. Funct. Imaging* **2010**, *30*, 308.
[23] A. A. Quyyumi, T. Crake, L. J. Mockus, C. A. Wright, A. F. Rickards, K. M. Fox, *Br. Heart J.* **1986**, *56*, 372.
[24] T. Vuorinen, K. Noponen, A. Vehkaoja, T. Onnia, E. Laakso, S. Leppänen, K. Mansikkamäki, T. Seppänen, M. Mäntysalo, *Adv. Mater. Technol.* **2019**, *0*, 1900246.
[25] K. E. Sandau, M. Funk, A. Auerbach, G. W. Barsness, K. Blum, M. Cvach, R. Lampert, J. L. May, G. M. McDaniel, M. V. Perez, S. Sendelbach, C. E. Sommargren, P. J. Wang, *Circulation* **2017**, *136*, e273.
[26] K. Nikus, J. Lähteenmäki, P. Lehto, M. Eskola, *J. Electrocardiol.* **2009**, *42*, 473.

[27] M. Mäntysalo, T. Vuorinen, V. Jeihani, A. Vehkaoja, in *Proc. SPIE – Int. Soc. Opt. Eng.*, **2017**.
[28] V. Jeyhani, T. Vuorinen, M. Mäntysalo, A. Vehkaoja, *Health Technol.* **2017**, *7*, 21.
[29] A. Aslam, A. Tiulpin, K. Noponen, T. Seppänen, *EMBEC & NBC 2017. EMBEC 2017, NBC 2017. IFMBE Proceedings*, Springer Singapore **2018**.
[30] J. S. Steinberg, N. Varma, I. Cygankiewicz, P. Aziz, P. Balsam, A. Baranchuk, D. J. Cantillon, P. Dilaveris, S. J. Dubner, N. El-Sherif, J. Krol, M. Kurpesa, M. T. La Rovere, S. S. Lobodzinski, E. T. Locati, S. Mittal, B. Olshansky, E. Piotrowicz, L. Saxon, P. H. Stone, L. Tereshchenko, G. Turitto, N. J. Wimmer, R. L. Verrier, W. Zareba, R. Piotrowicz, *Hear. Rhythm* **2017**, *14*, e55.